








A New One-Step Synthesis of Nanostructured Calcium Vanadate/Phosphate Apatite for Vanadate and Phosphorus Waste Valorisation: Characterization and Band Gap Determination

Fatima Zahra Chajri ¹, Meryem Bensemlali ¹, Hamid Nasrellah ^{1,2*}, Badreddine Hatimi ¹, Abdellatif Aarfane ^{1,2}, Mohamed Monkade ³, Jean-Michel Nunzi ⁴, Layla El Gaini ⁵, Mina Bakasse ¹

1 Faculty of Sciences, Laboratory of Organic Bioorganic Chemistry and Environment, Chouaib Doukkali University, El Jadida, Morocco

2 Higher School of Education and Training, Chouaib Doukkali University, El Jadida, Morocco

3 Physics of Condensed Matter Laboratory, Physics Department, Faculty of Science, Chouaib Doukkali University, El Jadida, Morocco

4 Queens University, Department of Chemistry, Department of Physics, Engineering Physics & Astronomy, Kingston, ON K7L-3N6, Canada

5 Laboratory of Applied Chemistry and Biomass, Faculty of Sciences Semlalia, Cadi Ayyad University, Marrakech, Morocco

* Correspondence: nasrellah.h@ucd.ac.ma

Scopus Author ID 57218168999

Received: 4.03.2023; Accepted: 12.04.2023; Published: 4.02.2024

Abstract: In this work, a series of vanadate-substituted hydroxyapatite (HAP) was directly prepared using a simpler, cost-effective, and one-step method. This proposed method involves mixing various contents of hydrated anhydrous gypsum with phosphoric acid, vanadium pentoxide, and sodium hydroxide. The reaction was conducted at room temperature for 48 h without needing pH adjustment. This method can be used with various ratios of starting compounds to produce both phosphate and vanadate apatites with high purity and yield and further investigate the formation of $\text{Ca}_{10}(\text{VO}_4)_x(\text{PO}_4)_{6-x}(\text{OH})_2$ ($x = 0, 1, 2, 3, 4, 5,$ and 6) structure. Indeed, two Moroccan solid wastes were used in this work: phosphorus gypsum (CaSO_4) was used as a source of calcium, while vanadium pentoxide (V_2O_5) was used as a source of vanadate. The synthesized apatite samples were characterized by X-ray diffraction (XRD) and analyzed by Fourier Transform Infrared Spectroscopy (FT-IR) to study their chemical composition and crystallinity. The optical properties of the prepared catalysts are determined by ultraviolet-visible spectroscopy (UV-vis). The morphological structures were investigated by scanning electron microscopy (SEM). The XRD analysis obtained showed that three crystalline phases were obtained successfully: vanadate apatite (VAP), HAP, and VAP-HAP mixture. These results were supported by FT-IR spectra. Besides, nanostructured materials with porosity were obtained for all samples. The samples presented a broad optical bandgap, providing a unique ribbon array that could block photo holes. Furthermore, the present method could greatly interest harmful waste recovery to synthesize new nanomaterials with intrinsic physicochemical properties.

Keywords: Vanadate hydroxyapatite, Hydroxyapatite, Nanomaterials, Catalyst, One-step method, Solid waste.

© 2024 by the authors. This article is an open-access article distributed under the terms and conditions of the Creative Commons Attribution (CC BY) license (<https://creativecommons.org/licenses/by/4.0/>).

1. Introduction

The source of vanadium pentoxide for apatite synthesis is the generated V_2O_5 waste for manufacturing sulfuric acid [1–3]. Vanadium has many industrial applications, and its contribution to environmental pollution continues to increase [4]. A three-step process involving oxidation and precipitation by acid leaching was used to recover vanadium pentoxide from a spent sulfuric acid catalyst [5]. Indeed, after precipitation with sulfuric acid, filtering, and drying, the fine and pointed sodium vanadate crystals appear very irritating to the nose, throat, and bronchi [1]. Because of its carcinogenicity, the International Programme on Chemical Safety (IPCS) states that vanadium pentoxide (V_2O_5) is a substance whose environmental emissions and concentrations may threaten human life, health, and the ecosystem. Furthermore, V_2O_5 meets the criteria for persistence but not for bioaccumulation [6,7].

The calcium source used for hydroxyapatite (HAP) synthesis is $CaSO_4$ waste from Morocco phosphorus gypsum containing calcium compounds, such as $CaSO_4$ anhydride or $CaSO_4$ hydrate [8–10]. Indeed, phosphorus gypsum is a by-product of phosphoric acid production and is a fundamental ingredient in the production of modern fertilizers. Calcium sulfate makes up the majority of phosphogypsum [10]. HAP is considered promising for the long-term containment of toxicants thanks to its environmental friendliness, excellent dispersibility, excellent stability, and variable surface functional groups [6,7]

On the other hand, catalysis has recently achieved a noteworthy development through many new applications. Catalysts are the main basis for the success and development of many new processes employed in several industrial fields [11]. Vanadium-based catalysts are the most used because they have suitable redox potential and Lewis's acid properties. However, substituting vanadate for phosphate is expected to result in a highly active oxidation catalyst and a unique acid-base catalyst [12,13]. The toxicity of elemental vanadium and its salts is well known [14]. In the aspect of optical applications, vanadium-based materials are widely used as photoelectrode materials due to their narrow bandgap, convenient band edge position, stability, and electrical properties [15–17]. It has been demonstrated that vanadium contribution in material synthesis can significantly tune the optical, band edge, and electrical properties [18]. The mechanism of vanadium incorporation in the human skeletal system may be supposed to be based on the isomorphous substitution of $(PO_4)^{3-}$ by $(VO_4)^{3-}$ in calcium phosphate apatite, $Ca_{10}(PO_4)_6(OH)_2$, abbreviated HAP [19,20]. In most studies, calcium HAP incorporated with $(VO_4)^{3-}$ HAP solid solutions, including vanadium, were investigated as a catalyst or in C–C bond-forming reactions [21,22]. To date, phosphate-based materials have been used as a catalyst for the oxidation of propane [23] and propargylic alcohol [24] and as a base catalyst [22] for the Michael reaction and the aldol condensation HAP solid solutions, including vanadium. Besides, vanadium-incorporated HAP has been shown to be attractive in the oxidation of numerous alkanes and alcohols [24–29].

Several traditional methods for HAP synthesis have been reported, including sol-gel [30,31], hydrothermal route [32], coprecipitation [33,34], and solid-state [35]. These methods are highly efficient in providing apatite materials of high purity, controlled size, and shape. Nonetheless, they are laborious, complex, and time-consuming, requiring skilled personnel and a high energy demand. Therefore, it is necessary to develop a simple synthesis method to overcome these limitations. In this context, the present study deals with substituting $(PO_4)^{3-}$ ions with $(VO_4)^{3-}$ ions using a one-step aqueous method. This synthesis method mainly

comprises two harmful wastes: phosphogypsum as a source of calcium and vanadium pentoxide as a source of vanadate. As far as we know, our proposed synthesis method was presented for the first time. It is based on mixing all reagents at one time at room temperature without any further aqueous additions and pH adjustment. Finally, it is worth noting that our method is straightforward, fast and cost-effective for providing HAP and VAP calcium nanoparticles in high yield. Furthermore, the present synthesis method could be promising in the valorisation of wastes (Phosphogypsum, vanadium pentoxide) which are harmful to the environment and human health.

2. Materials and Methods

2.1. Reagents and waste sources.

Phosphogypsum waste, as a source of calcium, used in this study was obtained from phosphorus gypsum in the town of El Jadida, Morocco. It is a grey, moist (5%), fine powder, silty sand material. The major component elements present in Moroccan phosphate are Ca (23.05 wt.%), S (18.04 wt.%), P (0.40 wt.%), and Fe (0.58 wt.%). Phosphorus gypsum was treated with sulfuric acid (67%), and the resulting composite was washed with water and then acetone before being dried at 65°C. Thereafter, the final product was sieved to obtain 40 μm anhydrous gypsum [8]. Vanadium pentoxide waste V₂O₅ was collected after the oxidation reaction of sulfur dioxide (SO₂) to sulfur trioxide (SO₃) involved in sulfuric acid manufacturing. H₃PO₄ and NaOH were purchased from Sigma-Aldrich (USA). NaOH was dissolved into 150 mL double distilled water at room temperature.

2.2. Preparation of vanadate-HAP Nanoparticles.

Figure 1 illustrates a schematic representation of the main experimental process used for nanosized HAP/VAP synthesis using phosphogypsum and vanadium pentoxide wastes as the main reactants of the coprecipitation reaction.

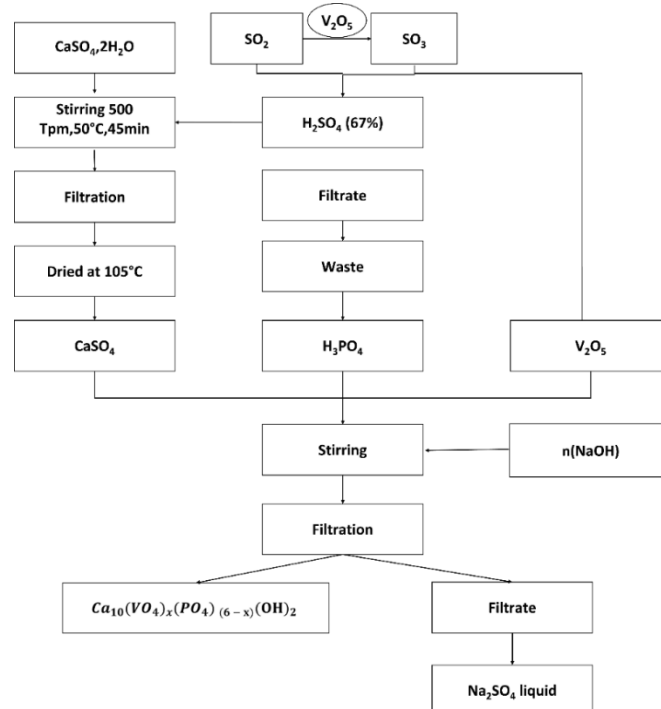
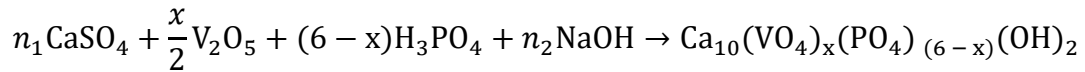


Figure 1. Schematic illustration of the main process followed for synthesizing nanosized HAP/VAP composite using phosphogypsum and vanadate waste.

A Serie of vanadate-HAP compositions $\text{Ca}_{10}(\text{VO}_4)_x(\text{PO}_4)_{(6-x)}(\text{OH})_2$ with x equal to 0, 1, 2, 3, 4, 5, 6 were synthesized by a simple coprecipitation method based on the following equation:



$(\text{VO}_4)^{3-}$ -incorporated calcium HAP was prepared using a mixture of different amounts of CaSO_4 , V_2O_5 , H_3PO_4 , and NaOH dissolved in 100 mL aqueous solution, as described in Table 1. Thereafter, the mixture was stirred using a mechanical shaker for 48 h at room temperature, as referred by our previously reported work [8]. The VAP/HAP produced was then removed from the solution by filtration, and the resulting powder was washed several times with water until a clear and neutral supernatant was obtained. Finally, solid samples were dried at 105 °C for 24 h and calcined at 900 °C for 3 h [36].

Table 1. Reagent quantities used to synthesize a nanosized HAP and VAP at different $(\text{VO}_4)^{3-}/(\text{PO}_4)^{3-}$ molar ratios according to the formula $\text{Ca}_{10}(\text{VO}_4)_x(\text{PO}_4)_{(6-x)}(\text{OH})_2$.

	CaSO₄	H₃PO₄	V₂O₅	NaOH	Xi
Quantity (mol)	0.073	0	0.022	0.001	X6
	0.073	0.007	0.018	0.022	X5
	0.073	0.014	0.014	0.044	X4
	0.073	0.021	0.010	0.066	X3
	0.073	0.029	0.007	0.087	X2
	0.073	0.036	0.003	0.109	X1
	0.073	0.043	0	0.131	X0

2.3. Physico-chemical techniques.

Different physicochemical techniques were used for the characterization of VAP/HAP nanocomposite. The prepared HAP/VAP nanocomposites were first characterized by the X-ray diffraction technique (X-ray Diffractometer (X-Pert Pro PAN analytical)). The Structural data obtained by X-ray diffraction analysis were characterized using INEL CPS (Curved Position Sensitive Detector) 120, operating with $\text{CuK}\alpha$ radiation ($K\alpha=1.54 \text{ \AA}$) at 40 kV and 30 mA. The analyzed sample was dried at room temperature (25 °C) for a period of 3 h. Besides, the surface morphology of all obtained solid samples was investigated using Scanning Electron Microscopy (Scanning Electron 103 Microscopy (SEM) (FEI Quanta 200 ESEM)). On the other hand, the chemical groups at the surface of the obtained HAP/VAP nanocomposites were identified by FT-IR (Nicolet 380 Fourier Transform Spectrometer). All solid samples were characterized according to Attenuated Total Reflectance (ATR) mode. Briefly, the procedure is to deposit a few grains on the diamond crystal of the ATR, and the analysis was carried out by using a Nicolet 380 Fourier Transform Spectrometer in a range of 4000 to 400 cm^{-1} wave-number with a resolution of 4 cm^{-1} . The optical measurements were performed using a UV–vis-NIR double-beam spectrophotometer SHIMADZU 3101 in the 300–1100 nm wavelength range.

3. Results and Discussion

3.1. XRD analysis.

The as-prepared nanocomposite samples, after being calcined at 900 °C for 3 h, the precipitate's XRD patterns were depicted in Figure 2. Seven samples of $\text{Ca}_{10}(\text{VO}_4)_x(\text{PO}_4)_{(6-x)}(\text{OH})_2$ ($x=0, 1, 2, 3, 4, 5,$ and 6) were set up for the current study. In the absence of vanadate groups, the XRD patterns of calcium HAP (Figure 2, $x=0$) matched the reference data for $\text{Ca}_{10}(\text{PO}_4)_6(\text{OH})_2$ (JCPDS 9-0423). For all samples, diffraction peaks appeared at nearly the same angle (2θ) values. When the x value changes from 0 to 6, the position of the XRD diffraction peaks continuously shifts to a tiny angular direction, and apatite phases with low vanadate content display broad peaks at higher diffraction angles. This could be attributed to the $(\text{VO}_4)^{3-}$ polyhedra's larger volume when compared to $(\text{PO}_4)^{3-}$, which was consistent with Boechat *et al.* [37], suggesting the formation of solid solutions of vanadate-HAP. As can be seen, each $\text{Ca}_{10}(\text{VO}_4)_x(\text{PO}_4)_{(6-x)}(\text{OH})_2$ XRD pattern ($x=0, 1, 2, 3, 4, 5,$ and 6) could be related to a specific crystallographic phase of an apatite structure [38–40]. The peaks also increase for intermediate x values at $x=3$, indicating the presence of both phosphate and vanadate ions in the lattice. Since there is no hydroxyl group, the diffraction peaks systematically decrease as x increases, which might be discussed as a sign of the absence of a hydroxyl group, suggesting the development of $\text{Ca}_{10}(\text{VO}_4)_x(\text{PO}_4)_{(6-x)}(\text{OH})_2$ nano-apatite. From XRD analysis, the final products exhibited good purity and characteristics that were coherent with other conventionally synthesized apatite materials.

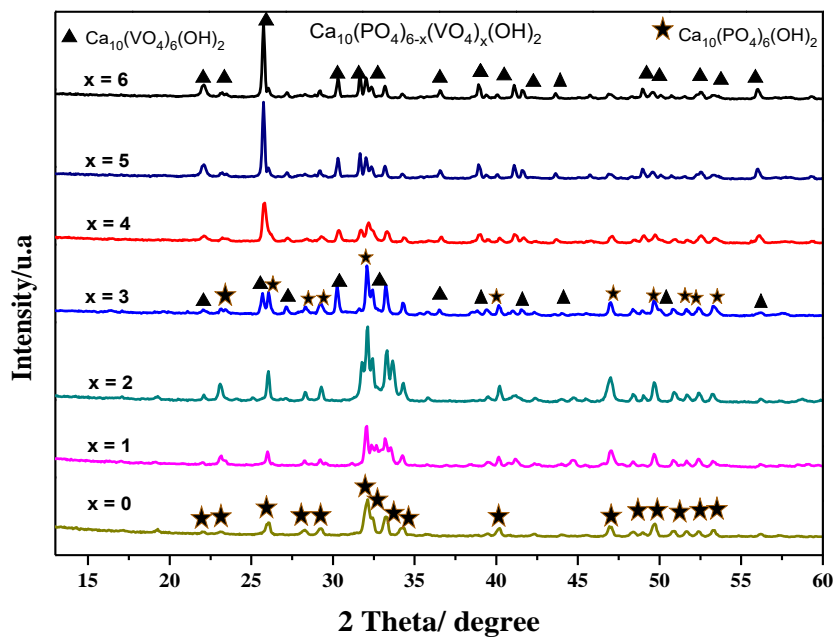


Figure 2. XRD spectra of $\text{Ca}_{10}(\text{VO}_4)_x(\text{PO}_4)_{(6-x)}(\text{OH})_2$ of ($x=0; 1; 2; 3; 4; 5; 6$) nano apatite after calcination at 900 °C for 3 h. The peaks labeled by ★ belong to $(\text{PO}_4)^{3-}$ and those marked by ▲ to $(\text{VO}_4)^{3-}$.

Using X-ray diffraction, the Scherrer formula has been frequently employed to calculate the dimensions of crystallites [41].

$$D = \frac{k\lambda}{\beta \cos\theta}$$

The full width at half maximum (FWHM) of samples calcined at 900 °C was evaluated. This parameter was frequently correlated with crystallite size, as demonstrated in Figure 3.

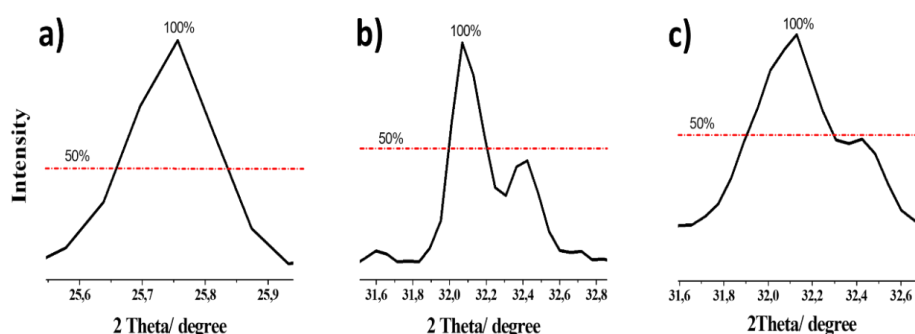


Figure 3. The width at half maximum of the high intense peak of nanosized HAP-VAP for (a) $x=0$, (b) $x=3$, (c) $x=6$ $\text{Ca}_{10}(\text{VO}_4)_x(\text{PO}_4)_{(6-x)}(\text{OH})_2$.

Table 2 summarizes crystalline parameter values obtained by applying the Scherrer formula, with $k=0.9$ and $\lambda=1.54056$ for $\text{Ca}_{10}(\text{VO}_4)_x(\text{PO}_4)_{(6-x)}(\text{OH})_2$. Indeed, the more vanadium content was incorporated into the apatite lattice, the less line width (β) will be, whereas the crystal size (D) increases. Furthermore, the crystallites found were on the nanometre scale. This lower crystallinity size is comparable to that shown for biological apatite in bone or dentin, which must not be overlooked. Hence, the proposed synthesis method in this work allows synthetic nanocrystalline apatite to be considered as a "model" that might replace biological apatite (e.g., for prosthesis application) [42].

Table 2. Values of crystal size of $\text{Ca}_{10}(\text{VO}_4)_x(\text{PO}_4)_{(6-x)}(\text{OH})_2$ nanocomposite based on the Scherrer formula.

X_i	θ (rad)	$\cos(\theta)$	β (rad)	D (nm)
X_6	0.225	0.974	0.003	46.914
X_4	0.225	0.975	0.005	26.147
X_3	0.281	0.961	0.008	17.305
X_0	0.280	0.961	0.008	16.138

3.2. FT-IR analysis.

Figure 4 exhibits FT-IR spectra of HAP/VAP, $\text{Ca}_{10}(\text{VO}_4)_x(\text{PO}_4)_{(6-x)}(\text{OH})_2$, nanocomposite prepared at different contents of vanadate and phosphate ($x = 0, 1, 2, 3, 4, 5, 6$). The FT-IR spectra show characteristic bands of $(\text{PO}_4)^{3-}$, $(\text{VO}_4)^{3-}$ and OH^- anions. It should be noted that absorption bands, located at around 1000 cm^{-1} , are all relatively sharp, which indicates that the final products were obtained with good crystallinity. Basically, two O-H stretching bands could appear in each spectrum; the first one, at approximately $3500\text{--}3600 \text{ cm}^{-1}$, and the second located at around $610\text{--}630 \text{ cm}^{-1}$ [32,43]. However, in the present study, it can be observed that no absorption bands corresponding to O-H vibration were observed in all infrared spectra in the wave number range located at around $3500\text{--}3600 \text{ cm}^{-1}$. This behavior could be attributed to ATR mode [44–47]. Meanwhile, the O-H stretching band appeared with only one peak and slightly shifted from 630 to 637 cm^{-1} with increasing the vanadate content. This slight change in terms of wave number could probably be due to vanadate substitution and/or incorporation in the apatite. In addition, this behavior, which corresponds to the OH group's hydrogen rotation, does not change appreciably with the vanadium content and is consistent with previously reported studies [19]. This vibration mode did not appear clearly for samples with $x=2, 3, 4, 5$, and 6 . The symmetric ν_1 and asymmetric ν_3 phosphate bands in the region of $895\text{--}1207 \text{ cm}^{-1}$ and ν_4 absorption bands in the region of $559\text{--}606 \text{ cm}^{-1}$ were observed

and were typical for the apatite structure (Figure 4). It has been reported that groups located at around 889-981 cm^{-1} can be attributed to V=O bonds. The groups around 806-889 cm^{-1} referred to the ν_3 (VO_4) modes, the band around 665-752 cm^{-1} due to the ν_3 ($\text{O}=\text{V}=\text{O}$) vibration mode, and groups around 554-608 cm^{-1} attributed to ν_1 ($\text{O}=\text{V}=\text{O}$) modes. Furthermore, it should be noted that ν_4 absorption bands related to phosphate were deformed with vanadate incorporation.

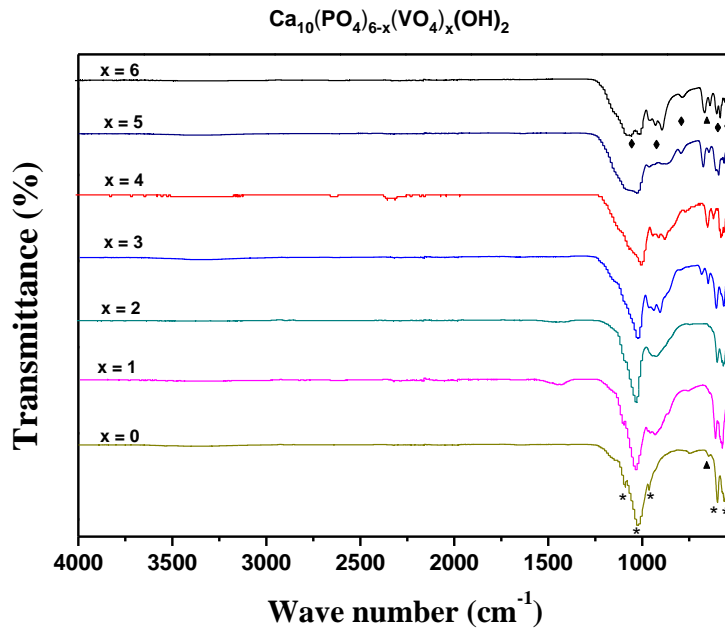


Figure 4. FTIR spectra of $\text{Ca}_{10}(\text{VO}_4)_x(\text{PO}_4)_{(6-x)}(\text{OH})_2$ of ($x=0, 1, 2, 3, 4, 5, 6$) nanoapatite after calcination at 900°C for 3h. The peaks labeled by (*) belong to $(\text{PO}_4)^{3-}$ and those marked by (◆) to $(\text{VO}_4)^{3-}$ and (▲) to (OH).

3.3. Optical properties.

The optical bandgap of the samples was calculated using the relation $(\alpha h\nu)^2 = A(h\nu - E_g)$ [48–50], where A is a constant, ν is the frequency of radiation, E_g is the bandgap, and α is the absorption coefficient. Figure 5 shows the extrapolation of the graph plotted between $(\alpha h\nu)^2$ and energy ($h\nu$). The UV-vis spectroscopic technique was used by performing linear range extrapolation to empirically determine the energy bandgap (E_g). As a complement to the energy bandgap determination, the calculated optical bandgap values were obtained to be 3.21, 3.16, and 3.05 eV for samples with $x = 0, x = 3,$ and $x = 6,$ respectively.

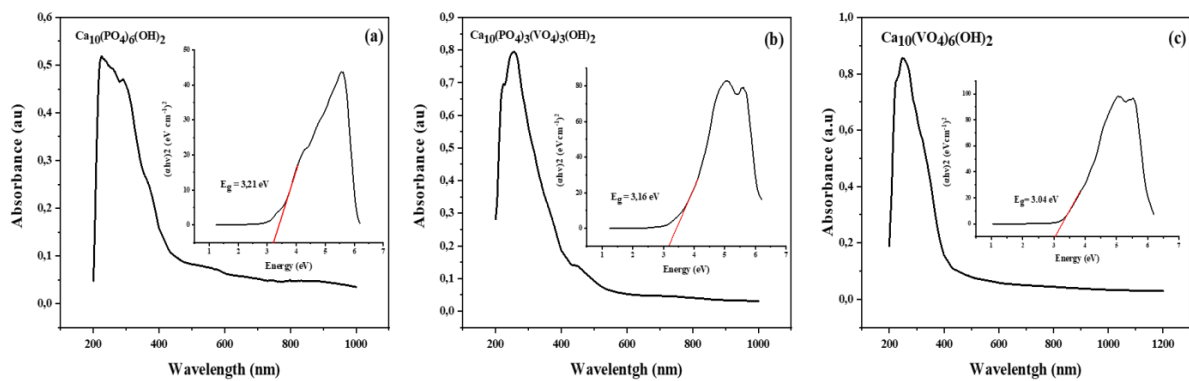


Figure 5. Absorbance spectra versus wavelength and energy bandgap of $\text{Ca}_{10}(\text{VO}_4)_x(\text{PO}_4)_{6-x}(\text{OH})_2$ apatite: (a) $x = 0,$ (b) $x = 3,$ (c) $x = 6.$

The optical bandgap value corresponding to the highest one (3.21 eV) was assigned to the fundamental bandgap of HAP. This was consistent with previous studies that found the energy bandgap of hydroxyapatite to be between 2.63 and 3.95 eV [51,52], which was also compatible with the value of HAP obtained. The values from direct gap calculations of E_g decrease with increasing vanadium content. The bandgap values of the samples obtained, as depicted in Figure 5, show that the vanadium ratio in the bandgap decreases with increasing vanadium content, which was generally related to the hydroxyapatite particle size. The XRD data analysis showed that the higher of the HAP composition, the larger the particle size will be. Furthermore, it was shown that the bandgap decreases with increasing grain size.

3.4. Morphological characterization.

Figure 6 shows morphological structures of the as-synthesized solid solutions, $\text{Ca}_{10}(\text{VO}_4)_x(\text{PO}_4)_{6-x}(\text{OH})_2$ ($x = 0, 1, 2, 3, 4, 5,$ and 6), with various vanadate/phosphate molar ratios at 900°C . It should be observed that the agglomeration and porosity were highly evident with increasing phosphate content and were probably attributed to Ostwald ripening and particle-particle repulsion [53]. On the other hand, an inhomogeneous structure of agglomerates was obtained when both phosphate and vanadate were present. This can probably be due to the non-uniformity in size and load between both species (phosphate and vanadate). Besides, the large crystals not homogeneously distributed might be due to the effect of the phosphate substitution with vanadate under synthesis conditions [54]. However, the sample $\text{Ca}_{10}(\text{VO}_4)_6(\text{OH})_2$ obtained at $x=6$ shows a highly homogeneous composition due to the uniform size of vanadate. The low porosity obtained could be due to the adaptability of our developed synthesis method to vanadate rather than phosphate synthesis.

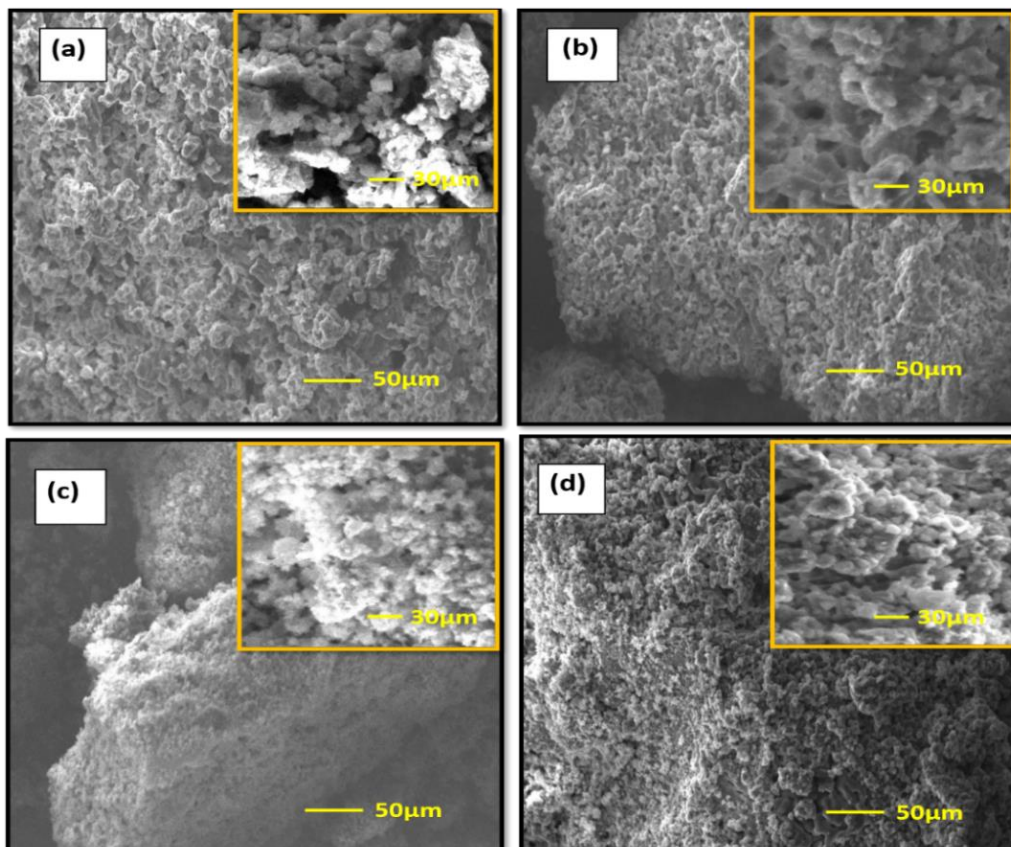


Figure 6. SEM images of $\text{Ca}_{10}(\text{VO}_4)_x(\text{PO}_4)_{6-x}(\text{OH})_2$ apatite: (a) $x=0$, (b) $x=3$, (c) $x=4$, (d) $x=6$.

4. Conclusions

In conclusion, a series of vanadate-substituted phosphate into the hydroxyapatite structure was successfully carried out by using a simple, cost-effective, and one-step coprecipitation synthesis method according to the following formula: $\text{Ca}_{10}(\text{VO}_4)_x(\text{PO}_4)_{6-x}(\text{OH})_2$. Moroccan phosphorus gypsum and vanadium pentoxide, two harmful solid wastes, were used as the main sources of calcium and vanadate, respectively. Hence, homogenous solid solutions of nanosized vanadate/phosphate hydroxyapatite were achieved at room temperature using this new proposed synthesis method, which did not require any further pH adjustment. Despite these advantages, the stability and size control of HAP/VAP particles still need to be investigated to determine which parameters are significantly related. Hence, surfactants would control the stability and size of the HAP/VAP particles. The crystallinity, homogeneity, and size findings were obtained using X-ray diffraction, SEM, and the Scherrer formula. In turn, the vibrational investigation exhibited that the VAP-HAP sample had an optical bandgap of 3eV. The prepared hydroxyapatite nanoparticles in this work have a big potential for further application (e.g., energy storage, semiconductors, etc.). In addition, the HAP/VAP nanocomposite could be used as an effective catalyst and/or adsorbent for pollutant removal from water samples (e.g., wastewater). Consequently, this method could be of great interest relative to other traditional synthesis methods for valorizing solid vanadium pentoxide wastes that cause serious environmental and human health problems.

Funding

This research received no external funding

Acknowledgments

The authors would like to greatly acknowledge the financial support and funding from the University of Chouaib Doukkali, El Jadida, Morocco.

Conflicts of Interest

Conflict of interest: The authors declare that there is no conflict of interest.

References

1. He, X.; Jarrell, Z.R.; Smith, M.R.; Ly, V.T.; Liang, Y.; Orr, M.; Go, Y.-M.; Jones, D.P. Metabolomics of V2O5 Nanoparticles and V2O5 Nanofibers in Human Airway Epithelial BEAS-2B Cells. *Toxicology and Applied Pharmacology* **2023**, *459*, 116327, <https://doi.org/10.1016/j.taap.2022.116327>.
2. Dakrouy, G.A.; El-Shazly, E.A.; Eliwa, A.A.; Mubark, A.E.; El-Azony, K.M. Utilization of Titanium Nanocomposites as Prospective Materials for Recycling of Vanadium (V) from Waste Solutions. *Journal of Molecular Liquids* **2022**, *366*, 120170, <https://doi.org/10.1016/j.molliq.2022.120170>.
3. Liu, J.; Huang, Y.; Li, H.; Duan, H. Recent Advances in Removal Techniques of Vanadium from Water: A Comprehensive Review. *Chemosphere* **2022**, *287*, 132021, <https://doi.org/10.1016/j.chemosphere.2021.132021>.
4. Nasimifar, A.; Mehrabani, J.V. A Review on the Extraction of Vanadium Pentoxide from Primary, Secondary, and Co-Product Sources. *International Journal of Mining and Geo-Engineering* **2022**, *56*, 361–382, <https://doi.org/10.22059/ijmge.2022.319012.594893>.
5. Khorfan, S.; Wahoud, A.; Reda, Y. Recovery of Vanadium Pentoxide from Spent Catalyst Used in the Manufacture of Sulphuric Acid. *Periodica Polytechnica Chemical Engineering* **2001**, *45*, 131–137, <https://pp.bme.hu/ch/article/view/281>.

6. Kulkarni, A.; Kumar, G.S.; Kaur, J.; Tikoo, K. A Comparative Study of the Toxicological Aspects of Vanadium Pentoxide and Vanadium Oxide Nanoparticles. *Inhalation Toxicology* **2014**, *26*, 772–788, <https://doi.org/10.3109/08958378.2014.960106>.
7. Costigan, M.; Cary, R.; Dobson, S.; Organization, W.H.; Safety, I.P. on C. *Vanadium Pentoxide and Other Inorganic Vanadium Compounds*; World Health Organization, **2001**, <https://apps.who.int/iris/handle/10665/42365>.
8. Nasrellah, H.; Yassine, I.; Hatimi, B.; Joudi, M.; Chema, A.; Gaini, L.E.; Hatim, Z.; Mhammedi, M.A.E.; Bakasse, M. New Synthesis of Hydroxyapatite from Local Phosphogypsum. *JMES* **2017**, *8*, 3168–3174, https://www.jmaterenvirosci.com/Document/vol8/vol8_N9/335-JMES-3173-Nasrellah.pdf.
9. Nasrellah, H.; Joudi, M.; Bensemlali, M.; Yassine, I.; Hatimi, B.; Hafdi, H.; Mouldar, J.; El Mhammedi, M.A.; Bakasse, M. Novel Synthesis and Characterization of Crystalline Fluorapatite from Moroccan Phosphogypsum Waste. *Matériaux & Techniques* **2022**, *110*, 102, <https://doi.org/10.1051/mattech/2022007>.
10. Bensemlali, M.; Joudi, M.; Nasrellah, H.; Yassine, I.; Aarfane, A.; Hatimi, B.; Hafdi, H.; Mouldar, J.; Bakasse, M. One-Step Synthesis and Characterisation of Crystalline Nano-Calcite from Phosphogypsum by Precipitation Method. *Eur. Phys. J. Appl. Phys.* **2022**, *97*, 50, <https://doi.org/10.1051/epjap/2022220041>.
11. Biedrzycka, A.; Skwarek, E.; Hanna, U.M. Hydroxyapatite with Magnetic Core: Synthesis Methods, Properties, Adsorption and Medical Applications. *Advances in Colloid and Interface Science* **2021**, *291*, 102401, <https://doi.org/10.1016/j.cis.2021.102401>.
12. Li, J.; Li, H.; Liu, Z.; Akri, M.; Tan, Y.; Kang, L.; Chi, J.; Qiao, B.; Ding, Y. Synergic Effect between Gold and Vanadate Substituted Hydroxyapatite Support for Synthesis of Methyl Methacrylate by One-Step Oxidative Esterification. *Chemical Engineering Journal* **2022**, *431*, 133207, <https://doi.org/10.1016/j.cej.2021.133207>.
13. Nowak, N.; Wiglusz, R.J. A Study of Vanadate Group Substitution into Nanosized Hydroxyapatite Doped with Eu³⁺ Ions as a Potential Tissue Replacement Material. *Nanomaterials* **2021**, *12*, 77, <https://doi.org/10.3390/nano12010077>.
14. Ali, M.M.S.; Imam, D.M.; El-Nadi, Y.A. Vanadium(V) Removal and Recovery by Adsorption onto Modified Activated Carbon Derived from Natural Hydroxyapatite. *J IRAN CHEM SOC* **2021**, *18*, 2771–2784, <https://doi.org/10.1007/s13738-021-02227-7>.
15. Kalanur, S.S.; Lee, Y.J.; Seo, H. Exploring the Synthesis, Band Edge Insights, and Photoelectrochemical Water Splitting Properties of Lead Vanadates. *ACS Appl. Mater. Interfaces* **2021**, *13*, 25906–25917, <https://doi.org/10.1021/acsami.1c03109>.
16. Abdi, F.F.; Berglund, S.P. Recent Developments in Complex Metal Oxide Photoelectrodes. *J. Phys. D: Appl. Phys.* **2017**, *50*, 193002, <https://doi.org/10.1088/1361-6463/aa6738>.
17. Gonçalves, J.M.; Ireno da Silva, M.; Angnes, L.; Araki, K. Vanadium-Containing Electro and Photocatalysts for the Oxygen Evolution Reaction: A Review. *J. Mater. Chem. A* **2020**, *8*, 2171–2206, <https://doi.org/10.1039/C9TA10857B>.
18. Darling, R.B.; Iwanaga, S. Structure, Properties, and MEMS and Microelectronic Applications of Vanadium Oxides. *Sadhana* **2009**, *34*, 531–542, <https://doi.org/10.1007/s12046-009-0025-x>.
19. Gruselle, M.; Tõnsuaadu, K.; Gredin, P.; Len, C. Apatites Based Catalysts: A Tentative Classification. *Molecular Catalysis* **2022**, *519*, 112146, <https://doi.org/10.1016/j.mcat.2022.112146>.
20. Sharfalddin, A.A.; Al-Younis, I.M.; Mohammed, H.A.; Dhahri, M.; Mouffouk, F.; Abu Ali, H.; Anwar, M.J.; Qureshi, K.A.; Hussien, M.A.; Alghrably, M. Therapeutic Properties of Vanadium Complexes. *Inorganics* **2022**, *10*, 244, <https://doi.org/10.3390/inorganics10120244>.
21. Kaneda, K.; Hara, T.; Hashimoto, N.; Mitsudome, T.; Mizugaki, T.; Jitsukawa, K. Creation of a Monomeric Vanadate Species in an Apatite Framework as an Active Heterogeneous Base Catalyst for Michael Reactions in Water. *Catalysis Today* **2010**, *152*, 93–98, <https://doi.org/10.1016/j.cattod.2009.08.018>.
22. Hara, T.; Kanai, S.; Mori, K.; Mizugaki, T.; Ebitani, K.; Jitsukawa, K.; Kaneda, K. Highly Efficient C–C Bond-Forming Reactions in Aqueous Media Catalyzed by Monomeric Vanadate Species in an Apatite Framework. *J. Org. Chem.* **2006**, *71*, 7455–7462, <https://doi.org/10.1021/jo0614745>.
23. Sugiyama, S.; Osaka, T.; Hashimoto, T.; Sotowa, K.-I. Oxidative Dehydrogenation of Propane on Calcium Hydroxyapatites Partially Substituted with Vanadate. *Catal Lett* **2005**, *103*, 121–123, <https://doi.org/10.1007/s10562-005-6513-7>.

24. Maeda, Y.; Washitake, Y.; Nishimura, T.; Iwai, K.; Yamauchi, T.; Uemura, S. Calcium Phosphate-Vanadate Apatite (CPVAP)-Catalyzed Aerobic Oxidation of Propargylic Alcohols with Molecular Oxygen. *Tetrahedron* **2004**, *60*, 9031–9036, <https://doi.org/10.1016/j.tet.2004.08.004>.
25. Ogo, S.; Onda, A.; Yanagisawa, K. Hydrothermal Synthesis of Vanadate-Substituted Hydroxyapatites, and Catalytic Properties for Conversion of 2-Propanol. *Applied Catalysis A: General* **2008**, *348*, 129–134, <https://doi.org/10.1016/j.apcata.2008.06.035>.
26. Sugiyama, S.; Osaka, T.; Hirata, Y.; Sotowa, K. Enhancement of the Activity for Oxidative Dehydrogenation of Propane on Calcium Hydroxyapatite Substituted with Vanadate. *Applied Catalysis A: General* **2006**, *312*, 52–58, <https://doi.org/10.1016/j.apcata.2006.06.018>.
27. Dasireddy, V.D.B.C.; Singh, S.; Friedrich, H.B. Oxidative Dehydrogenation of N-Octane Using Vanadium Pentoxide-Supported Hydroxyapatite Catalysts. *Applied Catalysis A: General* **2012**, *421–422*, 58–69, <https://doi.org/10.1016/j.apcata.2012.01.034>.
28. Dasireddy, V.D.B.C.; Singh, S.; Friedrich, H.B. Activation of N-Octane Using Vanadium Oxide Supported on Alkaline Earth Hydroxyapatites. *Applied Catalysis A: General* **2013**, *456*, 105–117, <https://doi.org/10.1016/j.apcata.2013.02.006>.
29. Dasireddy, V.D.B.C.; Singh, S.; Friedrich, H.B. Vanadium Oxide Supported on Non-Stoichiometric Strontium Hydroxyapatite Catalysts for the Oxidative Dehydrogenation of n-Octane. *Journal of Molecular Catalysis A: Chemical* **2014**, *395*, 398–408, <https://doi.org/10.1016/j.molcata.2014.08.044>.
30. Grayli, S.V.; Leach, G.W.; Bahreyni, B. Sol-Gel Deposition and Characterization of Vanadium Pentoxide Thin Films with High TCR. *Sensors and Actuators A: Physical* **2018**, *279*, 630–637, <https://doi.org/10.1016/j.sna.2018.07.002>.
31. Kalita, S.J.; Verma, S. Nanocrystalline Hydroxyapatite Bioceramic Using Microwave Radiation: Synthesis and Characterization. *Materials Science and Engineering: C* **2010**, *30*, 295–303, <https://doi.org/10.1016/j.msec.2009.11.007>.
32. Onda, A.; Ogo, S.; Kajiyoshi, K.; Yanagisawa, K. Hydrothermal Synthesis of Vanadate/Phosphate Hydroxyapatite Solid Solutions. *Materials Letters* **2008**, *62*, 1406–1409, <https://doi.org/10.1016/j.matlet.2007.08.087>.
33. Tsuchida, T.; Kubo, J.; Yoshioka, T.; Sakuma, S.; Takeguchi, T.; Ueda, W. Influence of Preparation Factors on Ca/P Ratio and Surface Basicity of Hydroxyapatite Catalyst. *J. Jpn. Petrol. Inst.* **2009**, *52*, 51–59, <https://doi.org/10.1627/jpi.52.51>.
34. Wu, Y.-S.; Lee, Y.-H.; Chang, H.-C. Preparation and Characteristics of Nanosized Carbonated Apatite by Urea Addition with Coprecipitation Method. *Materials Science and Engineering: C* **2009**, *29*, 237–241, <https://doi.org/10.1016/j.msec.2008.06.018>.
35. Parr, R.G.; Pearson, R.G. Absolute Hardness: Companion Parameter to Absolute Electronegativity. *J. Am. Chem. Soc.* **1983**, *105*, 7512–7516, <https://doi.org/10.1021/ja00364a005>.
36. Messing, G.L. Calcination and Phase Transformations. In *Encyclopedia of Materials: Science and Technology*; Elsevier, 2001; pp. 887–892 ISBN 978-0-08-043152-9, https://ui.adsabs.harvard.edu/link_gateway/2001emst.book..887M/doi:10.1016/B0-08-043152-6/00169-8.
37. Li, J.; Li, X.; Li, J.; Pu, X.; Wang, J.; Huang, Z.; Yin, G. Effects of Incorporated Vanadium and Its Chemical States on Morphology and Mesoporous Bioactive Glass Particles. *Microporous and Mesoporous Materials* **2021**, *319*, 111061, <https://doi.org/10.1016/j.micromeso.2021.111061>.
38. Bauer Boechat, C.; Eon, J.-G.; Malta Rossi, A.; Andre de Castro Perez, C.; Aguiar da Silva San Gil, R. Structure of Vanadate in Calcium Phosphate and Vanadate Apatite Solid Solutions. *Phys. Chem. Chem. Phys.* **2000**, *2*, 4225–4230, <https://doi.org/10.1039/b004339g>.
39. Petit, S.; Gode, T.; Thomas, C.; Dzwigaj, S.; Millot, Y.; Brouri, D.; Krafft, J.-M.; Rousse, G.; Laberty-Robert, C.; Costentin, G. Incorporation of Vanadium into the Framework of Hydroxyapatites: Importance of the Vanadium Content and PH Conditions during the Precipitation Step. *Phys. Chem. Chem. Phys.* **2017**, *19*, 9630–9640, <https://doi.org/10.1039/C6CP08782E>.
40. Patria, R.D.; Kumar, R.; Luo, L.; Varjani, S.; Wong, J.W.C.; Zhao, J. Exploiting an Efficient and Stable Catalyst for the Selective Oxidation of 5-Hydroxymethylfurfural to 2, 5-Diformylfuran by Incorporating Vanadium in the Framework of Hydroxyapatite. *ACS Sustainable Chemistry & Engineering* **2022**, *10*, 10514–10525, <https://doi.org/10.1021/acssuschemeng.2c01632>.
41. Scherrer, P. Bestimmung der inneren Struktur und der Größe von Kolloidteilchen mittels Röntgenstrahlen. In *Kolloidchemie Ein Lehrbuch*; Springer Berlin Heidelberg: Berlin, Heidelberg, 1912; pp. 387–409 ISBN 978-3-662-33517-8, <https://eudml.org/doc/59018>.

42. Shreyash, N.; Sonker, M.; Bajpai, S.; Tiwary, S.K. Review of the Mechanism of Nanocarriers and Technological Developments in the Field of Nanoparticles for Applications in Cancer Theragnostics. *ACS Applied Bio Materials* **2021**, *4*, 2307–2334, <https://doi.org/10.1021/acsabm.1c00020>.
43. Fowler, B.O. Infrared Studies of Apatites. I. Vibrational Assignments for Calcium, Strontium, and Barium Hydroxyapatites Utilizing Isotopic Substitution. *Inorg. Chem.* **1974**, *13*, 194–207, <https://doi.org/10.1021/ic50131a039>.
44. Vásquez Niño, A.F.; Santos, L.A.L. dos Preparation of an Injectable Macroporous α -TCP Cement. *Mat. Res.* **2016**, *19*, 908–913, <https://doi.org/10.1590/1980-5373-MR-2016-0229>.
45. Catauro, M.; Barrino, F.; Blanco, I.; Piccolella, S.; Pacifico, S. Use of the Sol–Gel Method for the Preparation of Coatings of Titanium Substrates with Hydroxyapatite for Biomedical Application. *Coatings* **2020**, *10*, 203, <https://doi.org/10.3390/coatings10030203>.
46. Roedel, E.; Urakawa, A.; Kureti, S.; Baiker, A. On the Local Sensitivity of Different IR Techniques: Ba Species Relevant in NO_x Storage-Reduction. *Phys. Chem. Chem. Phys.* **2008**, *10*, 6190, <https://doi.org/10.1039/b808529c>.
47. Kiefer, J.; Stärk, A.; Kiefer, A.; Glade, H. Infrared Spectroscopic Analysis of the Inorganic Deposits from Water in Domestic and Technical Heat Exchangers. *Energies* **2018**, *11*, 798, <https://doi.org/10.3390/en11040798>.
48. Johannes, A.Z.; Pingak, R.K.; Bukit, M. Tauc Plot Software: Calculating Energy Gap Values of Organic Materials Based on Ultraviolet-Visible Absorbance Spectrum. *IOP Conf. Ser.: Mater. Sci. Eng.* **2020**, *823*, 012030, <https://doi.org/10.1088/1757-899X/823/1/012030>.
49. Tauc, J. Optical Properties and Electronic Structure of Amorphous Ge and Si. *Materials Research Bulletin* **1968**, *3*, 37–46, [https://doi.org/10.1016/0025-5408\(68\)90023-8](https://doi.org/10.1016/0025-5408(68)90023-8).
50. Bui, D.-P.; Pham, M.-T.; Tran, H.-H.; Nguyen, T.-D.; Cao, T.M.; Pham, V.V. Revisiting the Key Optical and Electrical Characteristics in Reporting the Photocatalysis of Semiconductors. *ACS omega* **2021**, *6*, 27379–27386, <https://doi.org/10.1021/acsomega.1c04215>.
51. Rosenman, G.; Aronov, D.; Oster, L.; Haddad, J.; Mezinskis, G.; Pavlovska, I.; Chaikina, M.; Karlov, A. Photoluminescence and Surface Photovoltage Spectroscopy Studies of Hydroxyapatite Nano-Bio-Ceramics. *Journal of Luminescence* **2007**, *122–123*, 936–938, <https://doi.org/10.1016/j.jlumin.2006.01.331>.
52. Bystrov, V.S.; Piccirillo, C.; Tobaldi, D.M.; Castro, P.M.L.; Coutinho, J.; Kopyl, S.; Pullar, R.C. Oxygen Vacancies, the Optical Band Gap (E_g) and Photocatalysis of Hydroxyapatite: Comparing Modelling with Measured Data. *Applied Catalysis B: Environmental* **2016**, *196*, 100–107, <https://doi.org/10.1016/j.apcatb.2016.05.014>.
53. Arunseshan, C.; Suresh, S.; Arivuoli, D. Synthesis and Characterization of Nano-Hydroxyapatite (n-HAP) Using the Wet Chemical Technique. *International journal of physical sciences* **2013**, *8*, 1639–1645, <http://dx.doi.org/10.5897/IJPS2013.3990>.
54. Onda, A.; Ogo, S.; Kajiyoshi, K.; Yanagisawa, K. Hydrothermal Synthesis of Vanadate/Phosphate Hydroxyapatite Solid Solutions. *Materials Letters* **2008**, *62*, 1406–1409, <https://doi.org/10.1016/j.matlet.2007.08.087>.